Aggregated Model of Virtual Power Plants for Transient Frequency and Voltage Stability Analysis

Junru Chen, *Member, IEEE*, Muyang Liu, *Member, IEEE*, and Federico Milano, *Fellow, IEEE*

***Abstract*—The Virtual Power Plant (VPP) has been proposed to aggregate Distributed Generations (DGs) to act like a single power plant, thus, also has functions on the frequency and voltage support. The previous models of the VPP are static and focus on the energy trading and management. For the system transient response analysis, a dynamic VPP model must be needed. The paper proposes a reduced-order yet accurate aggregated model to represent VPP transients for the stability analysis of power systems. The goal is to provide a model that is adequate for system studies and can serve to the Transmission System Operator (TSO) to evaluate the impact of VPPs on the overall grid. The proposed model can accommodate the transient response of the most relevant controllers included in the distributed generators that compose the VPP. Using a comparison with a real-time detailed Electro-Magnetic Transients (EMT) models of the VPP confirms the validity of the proposed aggregated model. The case studies based on the IEEE 39-bus system verifies the accuracy of the proposed aggregated model on the system stability analysis.**

***Index Terms*—Frequency stability, voltage stability, fast frequency response (FFR), virtual power plant (VPP).**

I. Introduction

A. Motivation

IN THE context of the power system migrating into higher DG, the concept of the Virtual Power Plant (VPP) has been proposed to aggregate these DGs units and/or load, and to coordinate to act like a single power plant [1]. In order to maintain the system frequency and voltage stability, VPPs like any other power plants, are expected to have frequency and voltage support capabilities. However, the VPP consists of a number of DGs, each of which has its own transient response. A model able to represent the transient response of a VPP as a single dynamic device is sought by TSOs but still missing. This paper addresses this issue and proposes an aggregated VPP model for transient stability analysis.

Manuscript received July 13, 2020; revised December 11, 2020; accepted February 20, 2021. Date of publication March 3, 2021; date of current version August 19, 2021. The work of Junru Chen was supported by the European Commission, under the Project EdgeFLEX, under Grant 883710. The work of Muyang Liu and Federico Milano was supported by the Science Foundation Ireland, under Investigator Program under Grant SFI/15/IA/3074. The work of Federico Milano was supported by the European Commission under the Project EdgeFLEX, under Grant 883710 and under Investigator Program under Grant SFI/15/IA/3074. Paper no. TPWRS-01172-2020. *(Corresponding author: Muyang Liu.)*

Junru Chen and Muyang Liu were with the School of Electrical and Electronic Engineering, University College Dublin, 830046 Dublin, Ireland. They are now with the Xinjiang University, China (e-mail: junru.chen.1@ucdconnect.ie; muyang.liu@ucdconnect.ie).

Federico Milano is with the School of Electrical and Electronic Engineering, University College Dublin, 830046 Dublin, Ireland (e-mail: federico.milano@ucd.ie).

Color versions of one or more figures in this article are available at https://doi.org/10.1109/TPWRS.2021.3063280.

Digital Object Identifier 10.1109/TPWRS.2021.3063280

B. Literature Review

The vast majority of existing aggregated VPP models are aimed to solve the economic dispatch and energy management problems and are thus steady-state models [1], [2]. Instead, to date, the transient analysis of the high renewable system is based on the separated DG models. Based on their control, i.e. current sources or voltage sources, these DGs are classified into Grid-Following (GFL) and Grid-Forming (GFM) respectively [3]. References [4] and [5] propose a detailed full-order model for the GFL-DG and GFM-DG accordingly.

Since converter dynamics are fast with respect to the electromechanical modes and regulators of synchronous machines, the dominant dynamics of a DG comes from their controllers. Based on this observation, references [6] and [7] propose a 2nd-order model of the GFL-DG and GFM-DG. However, even with such second-order DG models, the computational burden may still be considerable if the number of units that compose the VPP is high. Moreover, from the viewpoint of a TSO, it is not viable to model the transient behavior of each small unit included in a VPP. TSOs, in fact, only need to know the transient response of the VPP as a whole.

Aggregating several small units into a simple(er) model is common practice. TSOs often employ aggregated grid models for dynamic security assessment. For example, the 179-bus Western Electricity Coordinating Council (WECC) system is aggregated from the original 10000+ bus transmission system. Fast frequency response analysis is based on the aggregated models, for example, reference [8] proposes a transfer function to aggregate all the synchronous generators and reference [9] proposes a generic transfer function to represent all of generations in the power system. For a more accurate frequency analysis in time domain simulation, reference [10] proposes a model to aggregate the multiple wind machine system into a single wind generator, reference [11] proposes method to aggregate the multiple grid-feeding converter system into a second order model and reference [12] proves that the virtual inertia response of the wind turbine can be aggregated into a similar form of the swing equation.

Most of the work interests on the system frequency response thus above models are based on the assumption that the voltage of the DG keeps constant. However, in reality, the occurrence

of any contingency disturbs the grid voltage and enforces the DG reaction on the voltage. The transient voltage regulation in the DG will affect its active power output and further affects the grid frequency. This interaction differs with the DG controls.

The DG works on the GFL mode and its voltage keeps constant. With regard to the VPP, it actually mixes GFL and GFM units with various frequency and voltage controls, so that its response is more involved. In order to model the entire VPP accurately, the system identification, such as inertia estimation [13] and grid impedance estimation [14], is required to determine the parameters of the aggregated model. To the best of the authors' knowledge, such a model has not been proposed so far.

C. Contributions

This work proposes an aggregated VPP model able to accurately reproduce the transient response of a VPP at the fundamental frequency for the transient frequency and voltage stability analysis. The secondary control of the VPP can ensure a solid output from all the internal DGs in the forthcoming commission period. The use case is to analyses the system response in the situation of the contingency occurrence, i.e. generator outage, load change and line outage. Thus, the aggregated model is based on the assumption that all the internal DG units working in unsaturated situation and working in the symmetrical situation. Since the units in a VPP can be either GFL or GFM, the proposed VPP model consists of a voltage source and a current source in parallel to emulate synchronization transients separately. The load in the VPP is modeled according to their location to minimize the effect of the voltage-dependent load on frequency and voltage response [15]. The proposed VPP model is verified via a fully-fledged Electro-Magnetic Transients (EMT) model and via a RMS transient stability model based on the IEEE 39-bus system.

D. Organization

The remainder of the paper is organized as follows. Section II reviews the basic concept of VPP and analyzes the transients of its internal units. Section III proposes the aggregated VPP model. Section IV validates the proposed aggregated model by comparing it with a detailed VPP EMT model in Matlab/Simulink. In Section V, the IEEE 39-bus system serves to show the accuracy of the proposed model for the system dynamic security assessment. Conclusions are drawn in Section VI.

II. Virtual Power Plant and Its Control

A VPP is a cluster of DGs with several different technologies, e.g. wind generator (WT), PV panels, electric vehicle (EV) chargers, electrical storage system (ESS) and loads as shown in Fig. 1. VPP can coordinate their internal units via the dual-directional communication system. The control tasks of the VPP are separated in its time scales, using threefold hierarchical layout including primary control, secondary control and tertiary control [16]. The latter two controls are centralized and implemented by Distribution System Operators (DSOs) and are not further considered in this work.

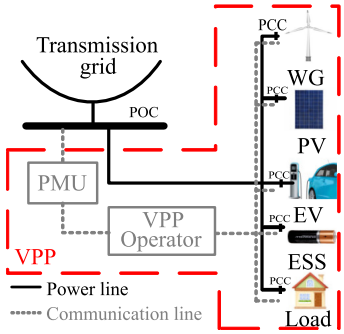

Fig. 1. VPP Structure.

The primary control, on the other hand, is implemented into the individual units to achieve fast frequency response, and primary frequency and voltage response. For the system dynamic security assessment by TSOs, the knowledge of the frequency and voltage supporting capabilities, the transient response and the grid power injection at the Point of Connection (POC) is required. The remainder of this section provides a brief review on the general DG control strategies, i.e. Grid-Following (GFL) and Grid-Forming (GFM).

A. Grid Following DG

The GFL-DGs is widely used in wind farms, PV plants and EV charger stations. It behaves like a current source, delivering the assigned current i_d, i_q or power p, q into the grid. Its grid synchronization is based on the voltage, using a Phase-Locked Loop (PLL) to track the phase of the voltage at the Point of Common Coupling (PCC). Note, PCC is a point of a single DG connecting to the rest of the VPP, while POC is a point of VPP connecting to the utility grid. Assuming that the phase angle of the PCC voltage is the reference, the phase of the VPP at the POC is $-\delta$. Then the q-axis PCC voltage in the synchronous dq-frame can be written as follows:

$$v_d = v_{\text{poc}} \cos(-\delta) - (\omega_g + \Delta\omega)\, l_g\, i_q\,, \tag{1}$$

$$v_q = v_{\text{poc}} \sin(-\delta) + (\omega_g + \Delta\omega)\, l_g\, i_d\,, \tag{2}$$

where ω_g is the grid frequency, $\Delta\omega$ is the PLL frequency deviation to the grid in transients, i.e. $\Delta\omega = \omega - \omega_g$, l_g is the grid inductance from the DG to the POC. The synchronization of the GFL-DG enforces v_q to be null as indicated in Fig. 2 and its time constant depends on the PI parameters, K_p, K_i normally in the range $[50, 100]$ ms [17]. Of course, there are advanced PLLs [18] for the purpose of lower harmonics, but essentially, they all contain a proportional part for a quick stabilization and an integral part for a zero steady-state error on the grid frequency deviations. Thus, here we use the generic PI-based PLL for simplicity.

When the converter is perfectly synchronized with the grid, the q-axis PCC voltage v_q is null while the d-axis PCC voltage v_d equals to the voltage magnitude at the POC. Moreover, the active power and reactive power are fully decoupled in the steady state or $v_q = 0$.

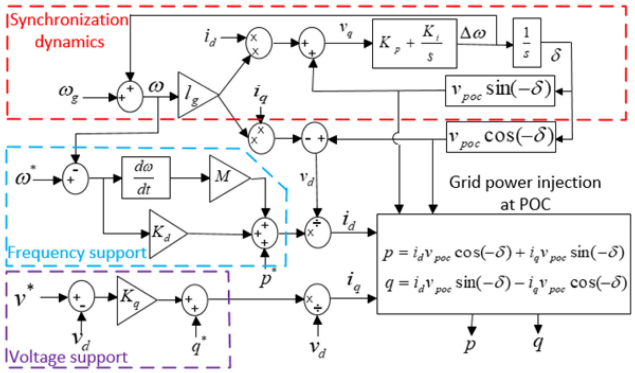

Fig. 2. GFL-DG dynamic model.

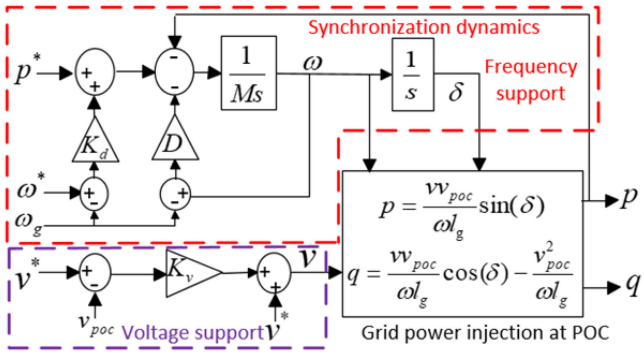

Fig. 3. GFM-DG dynamic model.

The reference currents of the converter control are given by:

$$i_d^{\mathrm{ref}} = \frac{p^{\mathrm{ref}}}{v_d}\,, \quad i_q^{\mathrm{ref}} = -\frac{q^{\mathrm{ref}}}{v_d}\,, \tag{3}$$

where the reference active and reactive powers are given by:

$$p^{\mathrm{ref}} = p^* + K_d(\omega^* - \omega) - M\,\dot{\omega}\,, \tag{4}$$

$$q^{\mathrm{ref}} = q^* + K_q(v^* - v_d)\,, \tag{5}$$

where ω^* and v^* are the nominal frequency and voltage, respectively. The active power reference (4) contains the feed-forward power p^* from the DC source of the DG and the power for the fast frequency response, i.e. df/dt response (inertia emulation) M, and the primary frequency control, i.e. *f-P* droop control K_d, where the frequency signal ω is is the grid frequency detected by the PLL or Phasor Measurement Unit (PMU); and the reactive power reference (5) contains the reactive power set point q^* and the compensated reactive power for the voltage support, i.e. the *V-Q* droop control K_q. Note, the virtual inertia in GFL could be achieved besides using ESS, the kinetic energy stored in turbine [19] and the de-loading control [20], but these all can be represented in the form of (4) [12].

The power delivered by the GFL-DG to the POC is:

$$p = i_d\, v_{\mathrm{poc}} \cos(-\delta) \;+\; i_q\, v_{\mathrm{poc}} \sin(-\delta)\,, \tag{6}$$

$$q = -i_q\, v_{\mathrm{poc}} \cos(-\delta) \;+\; i_d\, v_{\mathrm{poc}} \sin(-\delta)\,. \tag{7}$$

The resulting model of the GFL-DG is shown in Fig. 2, where the dynamics of the converter current controller have been neglected as their time scale is of the order of 1 ms and thus much faster than the synchronization dynamics and, hence, it has been assumed that $i_d = i_d^{\mathrm{ref}}$ and $i_q = i_q^{\mathrm{ref}}$ [6]. The computation of this GFL-DG reduced model includes 3 differential equations (two for PLL and one for RoCoF computation) and 7 algebraic equations.

B. Grid Forming DG

The GFM-DG is widely used in microgrids and is aimed at substituting the Synchronous Generator (SG) to impose the voltage and frequency to the grid. Its grid synchronization is based on the same principle as the SG, i.e. based on the power balance. A particular synchronization method for GFM-DGs is the Virtual Synchronous Generator (VSG), which consists in emulating the inertia through a swing equation. Again assuming that the PCC is the reference, the phase of the VPP at the POC is $-\delta$. Then the synchronization of the VSG is given by:

$$M\dot{\omega} = p - p^* + K_d(\omega^* - \omega_g) + D(\omega - \omega_g)\,, \tag{8}$$

where D is the damping coefficient. Note, the virtual inertia in GFM could be achieved besides using ESS, the power synchronization control [21] and DC voltage-based inertia emulation [22], but these all can be represented in the form of (8) [23]. The voltage support in the GFM-DG is a Automatic Voltage Regulation (AVR) with gain K_v as in SGs:

$$v = v^* + K_v(v^* - v_{\mathrm{poc}})\,. \tag{9}$$

Since the GFM-DG controls the voltage directly, its reactive power couples to the active power and the power at the POC is the consequence of the voltage difference between the PCC and POC. Assuming the system impedance is solely reactive, namely l_g, the power at the POC is:

$$p = \frac{v\, v_{\mathrm{poc}}}{\omega\, l_g}\, \sin(\delta)\,, \tag{10}$$

$$q = \frac{v\, v_{\mathrm{poc}}}{\omega\, l_g}\, \cos(\delta) - \frac{v_{\mathrm{poc}}^2}{\omega\, l_g}\,. \tag{11}$$

The dynamics of the converter voltage controller are of the order of 10 ms and are thus negligible. For the same reason, also the dynamics of the current controller are not considered, as in the model of the GFL-DG [7]. The resulting GFM-DG model is shown in Fig. 3. The computation of this GFM-DG reduced model includes 2 differential equations and 3 algebraic equations.

III. Aggregated VPP Model

As discussed above, the GFL-DG and GFM-DG have different dynamic responses. To properly capture their transients, thus, the proposed aggregated VPP model includes one current and one voltage source. Then, the distributed loads in a VPP can be represented with three aggregated loads, according to their locations as indicated in Fig. 4, where the impedance connecting to the POC is used to represent the effect of the VPP system impedance on the DG dynamics as shown in Fig. 2 and Fig. 3.

Note that, in steady-state, since the GFL-DGs controls active and reactive power directly, the aggregated current source

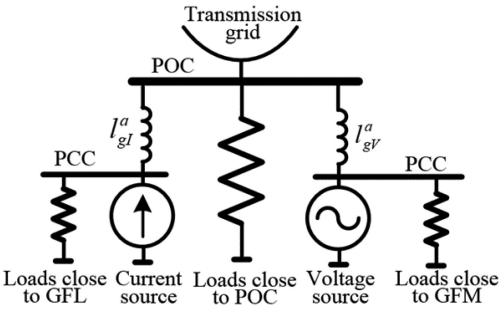

Fig. 4. VPP equivalent model.

is modelled as PQ bus with negative powers; whereas, since GFM-DGs controls the active power and the voltage directly, the aggregated voltage source model is modelled as a PV bus.

The remainder of this section discusses the definition of the parameters of the aggregated VPP model shown in Fig. 4.

A. Aggregated Current Source Model

Let us assume that the VPP includes n GFL-DGs. Taking the POC as the observation point, these GFL-DGs can be represented by a Norton equivalent circuit where the n current sources are connected in parallel. The resulting aggregated model can be easily obtained as the sum of their currents and multiple of their impedances, as follows:

$$i_d^{\mathrm{a}} = \frac{\sum_{i=1}^n p_i^* + \sum_{i=1}^n \Delta p_i}{v_d}\,, \tag{12}$$

$$i_q^{\mathrm{a}} = -\frac{\sum_{i=1}^n q_i^* + \sum_{i=1}^n \Delta q_i}{v_d}\,, \tag{13}$$

and

$$\frac{1}{l_{g\mathrm{I}}^{\mathrm{a}}} = \sum_{i=1}^n \frac{1}{l_{g,i}}\,, \tag{14}$$

where, Δp_i (Δq_i) is the active (reactive) power compensation of the GFL-DG i for the frequency (voltage) support. Considering the power compensation from each GFL is (4) and (5), the total power compensation can be computed as:

$$\sum_{i=1}^n \Delta p_i = \sum_{i=1}^n K_{d,i}(\omega^* - \omega_i) - \sum_{i=1}^n M_i \dot{\omega}_i\,, \tag{15}$$

$$\sum_{i=1}^n \Delta q_i = \sum_{i=1}^n K_{q,i}(v^* - v_{\mathrm{poc}})\,, \tag{16}$$

where we assume that the set points ω^* and v^* are the same for all GFL-DGs. In turn, the *f-P* gain, Rate of Change of Frequency (RoCoF) gain and *V-Q* gain of the aggregated current source are the sum of the values of all GFL-DG included in the VPP.

The synchronism difference of the GFL-DGs mainly depends on the term $l_g i_d$ in Fig. 2. The larger $l_g i_d$, the longer the synchronizing dynamics, in fact, the feed-forward loop of the GFL-DG synchronizing dynamics depends on $l_g i_d(K_p + \frac{K_i}{s})$. Based on this observation, the aggregated PLL parameters can be computed as the weighted sum of the PI parameters of all GFL-DGs in the VPP as indicated in (17). Since $i_{d,i}$ in reality is variable, for simplicity, in the computation of the synthetic PLL parameter, assuming the active and reactive power is decoupled, the active current then can be represented by the active power reference as follows:

$$\begin{aligned} K_p^{\mathrm{a}} + \frac{K_i^{\mathrm{a}}}{s} &= \frac{\sum_{i=1}^n l_{g,i} i_{d,i}(K_{p,i} + \frac{K_{i,i}}{s})}{\sum_{i=1}^n l_{g,i} i_{d,i}} \\ &\approx \frac{\sum_{i=1}^n l_{g,i} p_i^*(K_{p,i} + \frac{K_{i,i}}{s})}{\sum_{i=1}^n l_{g,i} p_i^*}\,. \end{aligned} \tag{17}$$

Substituting the synthetic parameters i_d^{a}, i_q^{a}, l_g^{a}, K_p^{a} and K_i^{a} into Fig. 2, we obtain the aggregated current sources and (1), (2) and (12)-(7) constitute the resulting Differential-Algebraic Equation (DAE) model of the aggregated current source.

B. Aggregated Voltage Source Model

Let us assume that the VPP includes m GFM-DGs. Taking the POC as the observation point, the GFM-DGs can be represented by a Thevenin equivalent circuit where the m voltage sources are connected in parallel. The resulting aggregated model is a voltage source connected to the POC through a line. The active power of the aggregated voltage source is the sum of the active powers of all GFM-DGs:

$$p^{\mathrm{a}} = \sum_{i=1}^m p_i \approx v_i v_{\mathrm{poc}} \sin\delta_i \sum_{i=1}^m \frac{1}{\omega_o l_{g,i}}\,, \tag{18}$$

where, for simplicity the ω_i's of the GFM-DGs have been approximated as the reference angular speed, namely $\omega_i \approx \omega_o$. Similarly, the reactive power at the POC is given by:

$$q^{\mathrm{a}} = \sum_{i=1}^m q_i \approx v_i v_{\mathrm{poc}} \cos\delta_i \sum_{i=1}^m \frac{1}{\omega_o l_{g,i}} - v_{\mathrm{poc}}^2 \sum_{i=1}^m \frac{1}{\omega_o l_{g,i}}\,. \tag{19}$$

From (18) and (19), the aggregated line impedance $l_{g\mathrm{V}}^{\mathrm{a}}$ of the aggregated voltage source is computed similarly by (14) using all the Thevenin equivalent impedance of the GFM-DGs. Then, substituting (9) into (11) and (19), we obtain the reactive power due to the voltage change ($\Delta v = v^* - v_{\mathrm{poc}}$) at the POC as follows:

$$\Delta q^{\mathrm{a}} = \Delta v \sum_{i=1}^m \frac{K_{v,i}\cos\delta_i}{\omega_o l_{g,i}}\,, \tag{20}$$

where, again $\omega_i \approx \omega_o$, $\forall i = 1,\ldots,m$. Finally, the aggregated AVR gain K_v^{a} is computed as the weighted sum of the AVR gain $K_{v,i}$ of all GFM-DGs:

$$K_v^{\mathrm{a}} = \frac{\sum_{i=1}^m (K_{v,i}\cos(\delta_i)/\omega_o l_{g,i})}{\sum_{i=1}^m \cos(\delta_i)/\omega_o l_{g,i}} \approx \frac{\sum_{i=1}^m K_{v,i}\, q_i}{\sum_{i=1}^m q_i}\,. \tag{21}$$

As shown in Fig. 3, the dynamics of the frequency response and synchronization are in the same loop, whose dynamic behavior is determined by the inertia, damping and droop coefficients. The inertia M^{a} and droop K_d^{a} of the aggregated voltage source is simply the sum of inertias and droops of all GFM-DGs:

$$M^{\mathrm{a}} = \sum_{i=1}^m M_i\,, \qquad K_d^{\mathrm{a}} = \sum_{i=1}^m K_{d,i}\,. \tag{22}$$

The equivalent angular speed (frequency) of the aggregated voltage source is obtained as weighted sum of the frequencies of all GFM-DGs, similarly to the concept of the Center of Inertia (CoI), as follows:

$$\omega = \frac{\sum_{i=1}^{m} M_i \omega_i}{\sum_{i=1}^{m} M_i} . \tag{23}$$

The synthetic damping within VPP consists of the damping in the DGs and the losses from the VPP grid resistances, thus, cannot be simply computed as the sum of the damping coefficients of the GFM-DGs. Essentially, damping is the friction power to prevent the frequency change. Based on this, we propose to compute the damping through the swing equation (8), as follows:

$$D^{\mathrm{a}} = \frac{\sum_{i=1}^{m} p_i - p^* - K_d^{\mathrm{a}}(\omega^* - \omega) + \dot{\omega} M^{\mathrm{a}}}{\omega - \omega_g} . \tag{24}$$

Substituting the synthetic parameters K_v^{a}, M^{a}, K_d^{a} and D^{a} into the scheme represented in Fig. 3, we obtain the aggregated voltage source. Equations (8), (9) and (18)-(24) constitute the resulting DAE model of the aggregated voltage source.

C. Load

The GFL- or GFM-interfaced loads can be modelled and aggregated into previous current or voltage source model respectively with negative generation. While other l loads are generally modelled as voltage-dependent load:

$$p_{l,i} = p_{l0,i} \left(\frac{v_i}{v^*}\right)^{\alpha_i}, \qquad q_{l,i} = q_{l0,i} \left(\frac{v_i}{v^*}\right)^{\beta_i} . \tag{25}$$

Where α_i/β_i is the voltage coefficient of the active/reactive power. When $\alpha_i = \beta_i = 0$, it is constant power loads, $\alpha_i = \beta_i = 1$, it is constant current loads, $\alpha_i = \beta_i = 2$, it is constant impedance loads. Loads are distributed in the region of the VPP and we assume that their voltage depends on the nearby DG. GFL-DGs control the power directly, while its terminal voltage is passively controlled as the consequence of the the assigned power set point. On the other hand, GFM-DGs control the voltage directly. Based on these observations, loads can be classified into three categories, according to the location:

i) v_i is set to the voltage at the POC if the load is closed to the POC;
ii) v_i is set to the voltage of the aggregated current source output if the load is closed to the GFL-DG;
iii) v_i is set to the voltage of the aggregated voltage source output if the load is closed to the GFM-DG;

Then, the distributed loads are aggregated into three clusters, namely at the buses of the POC, current source and voltage source, respectively, as shown in 4. Note that, in reality, v_i is not exactly equal to the aggregated bus voltage. Hence a small mismatch on the loading is inevitable.

D. System Identification

A VPP generally measures $(v_i, i_{d,i}, i_{q,i})$ or (p_i, q_i, ω_i) at the terminal of each DG, and commands the set-point p_i^*, q_i^*, v^*, ω^* and the primary control gains $K_{d,i}$, $K_{q,i}$, $K_{v,i}$ to each DG according to the unit commitment of its secondary control.

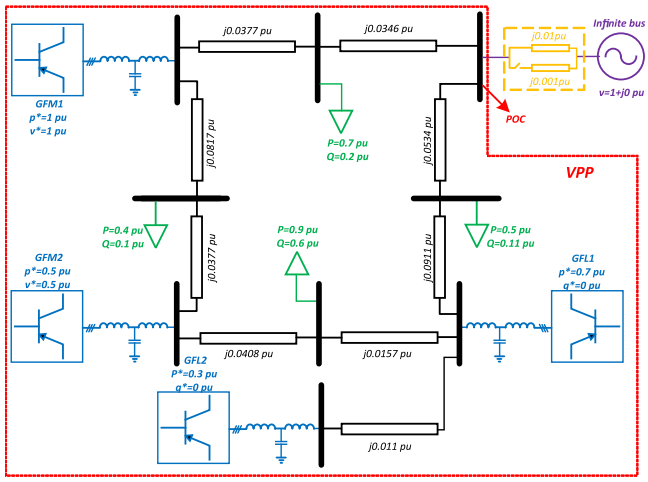

Fig. 5. VPP topology for EMT simulation.

However, the internal dynamic parameters, inertia M_i, input inductance $l_{g,i}$ and damping D_i are not known by the VPP. For example, some of DGs use the adaptive and alternating inertia, and some feed forward the inertia of the turbine for the grid inertia provision. In the aggregated model, the damping can be identified with (24) but the inertia M_i and input impedance $l_{g,i}$ still need to be identified. The power system identification is a broad topic and still under researching. There are many methods in the literature. Here we only introduce one method based on [24]:

$$\dot{M}_i = T_{m,i}(\Delta P_i - K_{d,i}(\omega_i^* - \omega_i) - M_i \dot{\omega}_i)\mathrm{sign}(\dot{\omega}_i) . \tag{26}$$

where $T_{m,i}$ is the time constant of the inertia estimation.

The system reactance from each DG to POC can be computed via a derivation of the power flow equation (10) [25], [26]:

$$l_{g,i} = \frac{v_i v_g \sin(\delta_i)}{\Delta p_i} \approx \frac{v_i v_g \int(\omega_i - \omega_g)}{\Delta p_i} . \tag{27}$$

The aggregated VPP model is completed. In comparison with a VPP full model, the construction of the model from $3n + 2m$ differential equations plus $7n + 3m + 2l$ algebraic equations is reduced to 5 differential equations plus 16 algebraic equations. The larger number of the units in the VPP, the larger computational relief using the aggregated model.

IV. Model Validation

A real-time simulation solved in Matlab/Simulink is utilized to validate the proposed aggregation model against fully-fledged EMT models that represent each element of the VPP. The tested VPP is shown in Fig. 5. It consists of 2 GFL-DGs, 2 GFM-DGs and 4 loads connected to an infinite bus. This infinite bus is modelled as an ideal voltage source, with controlled frequency and voltage. The nominal frequency is 50 Hz. The base voltage is 10 kV and base power is 1 MW. The DG parameters as well as the aggregated voltage/current source model settings are given in Table I. For simplicity, the converter parameters are the same for all DGs and are given in Table II. The system parameters

TABLE I
DGs AND AGGREGATED MODEL PARAMETERS

Unit	M [MWs/rad]	K_d [MW/rad]	D [MW/rad]	K_v/K_q	l_g [H]
GFL1	1.0	110	-	600	0.157
GFL2	1.5	80	-	367	0.193
GFM1	0.6	50	50	0.9	0.135
GFM2	0.3	80	80	0.9	0.160
I-model	2.5	190	-	967	0.087
V-model	0.9	130	163	0.9	0.066

TABLE II
CONVERTER PARAMETERS OF DGs

Parameter	Value	Parameter	Value
LCL filter (μH/L)	0.5/3/0.1	Voltage controller P/I	0.01/10.4
Current controller P/I	5000/10400	GFL1 PLL P/I	144/2560
GFL2 PLL P/I	126/2240	I-model PLL P/I	138/2450

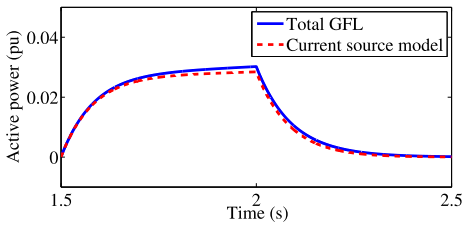

(a) GFL-DGs vs. aggregated current source model.

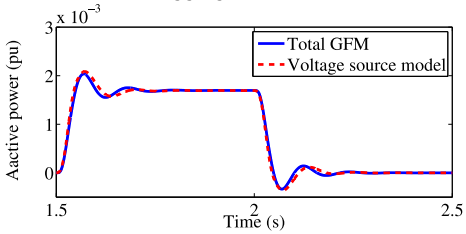

(b) GFM-DGs vs. aggregated voltage source model.

Fig. 6. Active power transient response after a frequency variation.

are shown in Fig. 5. The perturbances are a voltage change and frequency change of the ideal source.

A. Transient Response Following Frequency Variations

This section verifies the accuracy of the aggregated model in response to a frequency change at the POC. The initial steady-state is characterized by 50 Hz frequency and 1 pu voltage at the POC. At $t = 2$ s, the frequency of the ideal source starts decreasing from 50 Hz s to 49.85 Hz with a 0.3 Hz/s slope. The frequency variation stops at 2.5 s. For simplicity and to better illustrate the dynamics, the results below only show the fast frequency response.

Figure 6 shows the comparison of the active power transients between the total power of the GFL-DGs (GFM-DGs) of the detailed model and the aggregated current (voltage) source. The aggregated models appears to capture accurately the dynamics of the overall VPP.

Figure 7 shows the results of the reactive power transients between the detailed VPP and the proposed aggregated model. Both the detailed VPP and the aggregated model present a

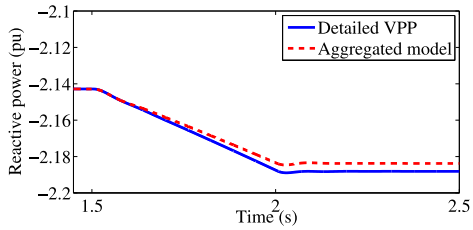

Fig. 7. Reactive power transient response after a frequency change.

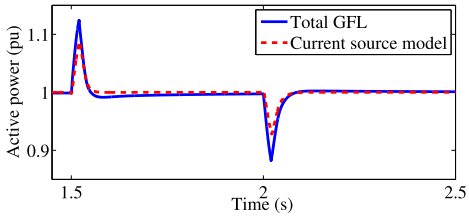

(a) GFL-DGs vs. aggregated current source model.

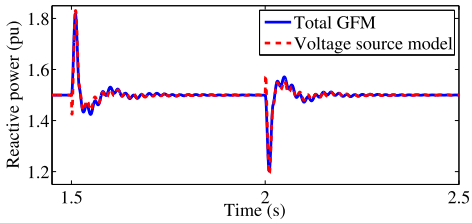

(b) GFM-DGs vs. aggregated voltage source model.

Fig. 8. Active power transient response after voltage variations.

reduction of the reactive power. This reduction is due to the power coupling of the GFMs and the voltage dependent loads. Although the voltage level of the aggregated voltage source is set to match the initial reactive power of the detailed model, local GFM-DG voltages may be different in the detailed VPP model. Consequently, the reactive power response can show some small difference in the two models, as illustrated in (19). Similarly, as mentioned above, the aggregated load voltage may be different from the local voltages of the actual loads. These are the reasons why Fig. 7 shows a reactive power mismatch between the aggregated model and the detailed VPP. However, since the voltage differences in the GFM-DGs and/or in the load are generally small, such a mismatch is negligible.

B. Transient Response Following Voltage Variations

This section verifies the accuracy of the aggregated model in response to voltage step variations. The initial steady-state is characterized by 50 Hz frequency and 1 pu voltage at the POC. The voltage of the ideal source jumps from 1 pu to 0.9 pu at $t = 2$ s and recovers to 1 pu at $t = 2.5$ s.

Figure 8 shows the active power transients following the voltage variations. The dynamic response of the GFL-DGs show two aspects: (i) the negative feedback of the PLL synchronization; and (ii) the reactive power compensation. Because of these effects, the active and reactive powers of the GFL-DG are coupled during the transient. This leads to the spike in the active power at the instant of the voltage change. The aggregated model

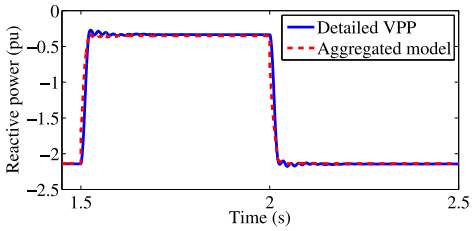

Fig. 9. Reactive power transient response after voltage variations.

shows a lower peak on the active power than the detailed VPP, because it neglects the transients of the current controller.

With regard to the GFM-DGs, the steps in the voltage activates the AVR that, as a consequence, increases the output voltage of the DGs. This voltage regulation leads to the active power change as indicated in (18). Then the power synchronization of the GFM-DG moves the phase to re-track its power reference. This transient behavior is well reflected in the aggregated voltage source model. The sub-transient oscillation is due to the dynamic coupling between the swing equation and the system impedance [27]. This behavior is also accurately captured by the aggregated model.

Figure 9 shows the reactive power transient of the detailed and aggregated VPPs. The voltage support of the VPP compensates the reactive power following the POC voltage change. The aggregated model accurately captures such a reactive power compensation. Since the grid voltage before $t = 2$ s and after $t = 2.5$ s is the same, the reactive power trajectories at post fault are perfectly matched. However, during the POC voltage sag, there is a small mismatch due to the different voltage levels in the VPP grid. Again, this mismatch is small and does not affect the overall accuracy of the aggregated model.

C. Transient Response Following Grid Impedance Variation

This section verifies the accuracy of the aggregated model in response to the grid impedance variation. The infinite bus now connects to the VPP via a parallel transmission line, of which value is 0.01 pu and 0.001 pu. The line of 0.001 pu is cut off at 2 s.

Figure 10 shows the active power transients following the line outage. The aggregated model can basically capture the response of the VPP, but shows a higher mismatches for the aggregation of the GFL-DGs. This is because the phase at this time is jumped at the POC and the grid impedance increases. This lead to the transient current in the GFL-DGs lower its reference, thus, resulting in a less peak than the aggregated model with reference current output.

Figure 11 shows the reactive power transients following the line outage. Since GFL-DGs applies the constant power control, the reactive power variation is insignificant, only in the order of $10^{-}3$ pu. The aggregated current source model captures the synchronous resonance occurred in the GFL-DGs. On the other hand, the grid impedance change leads to the reactive power change in the GFM-DGs and this is well represented by the voltage source model as indicated in (20).

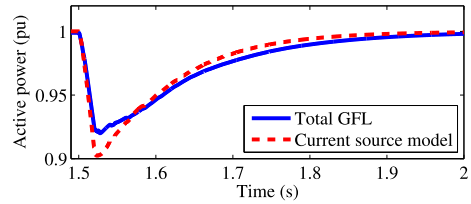

(a) GFL-DGs vs. aggregated current source model.

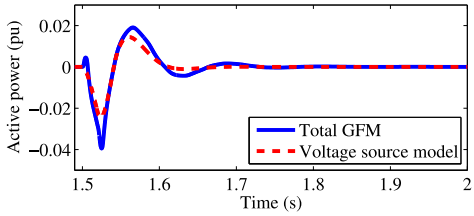

(b) GFM-DGs vs. aggregated voltage source model.

Fig. 10. Active power transient response after line outage.

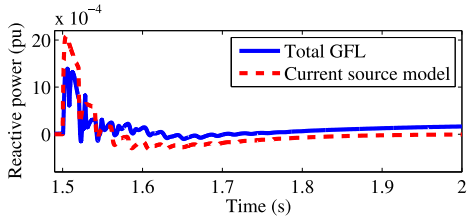

(a) GFL-DGs vs. aggregated current source model.

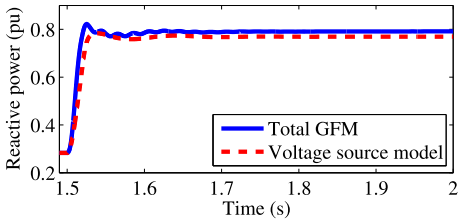

(b) GFM-DGs vs. aggregated voltage source model.

Fig. 11. Reactive power transient response after line outage.

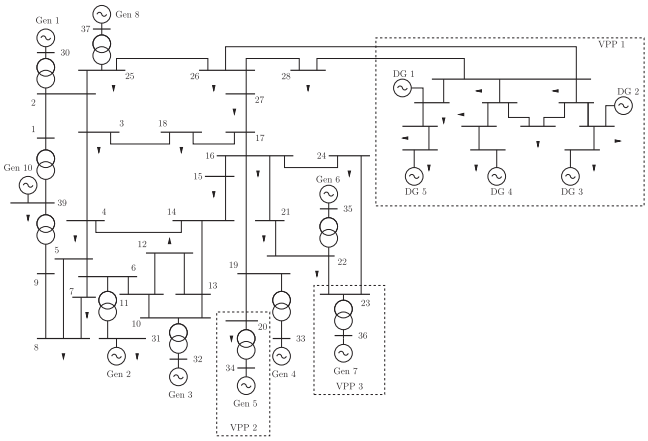

Fig. 12. VPPs in the modified New England system.

TABLE III
VPPs AND ITS AGGREGATION MODEL PARAMETERS

Unit	M	K_d	D	K_v/K_q	$l_g\,\omega$
VPP1-GFL1	0	35	-	100	$1.12 \cdot 10^{-3}$
VPP1-GFL2	20	52	-	88	$6.99 \cdot 10^{-4}$
VPP1-GFL3	45	44	-	65	$6.89 \cdot 10^{-4}$
VPP1-GFM1	20	35	35	0.9	$2.17 \cdot 10^{-4}$
VPP1-GFM2	42	50	50	0.9	$9.86 \cdot 10^{-4}$
VPP1-I-model	65	131	-	253	$2.65 \cdot 10^{-4}$
VPP1-V-model	62	85	85	0.9	$6.38 \cdot 10^{-3}$
VPP2-GFL1	21	46	-	73	$4.97 \cdot 10^{-4}$
VPP2-GFL2	10	82	-	81	$7.25 \cdot 10^{-4}$
VPP2-GFL3	0	44	-	37	$2.75 \cdot 10^{-3}$
VPP2-GFM1	75	55	55	0.9	$8.78 \cdot 10^{-4}$
VPP2-GFM2	52	34	34	0.9	$6.39 \cdot 10^{-3}$
VPP2-I-model	31	172	-	191	$2.66 \cdot 10^{-4}$
VPP2-V-model	127	89	89	0.9	$6.69 \cdot 10^{-3}$
VPP3-GFL1	15	36	-	23	$1.09 \cdot 10^{-3}$
VPP3-GFL2	18	22	-	31	$1.32 \cdot 10^{-3}$
VPP3-GFL3	8	19	-	17	$2.48 \cdot 10^{-3}$
VPP3-GFM1	31	42	42	0.9	$2.02 \cdot 10^{-3}$
VPP3-GFM2	27	18	18	0.9	$1.56 \cdot 10^{-3}$
VPP3-I-model	41	77	-	71	$4.81 \cdot 10^{-4}$
VPP3-V-model	58	60	60	0.9	$9.45 \cdot 10^{-3}$

V. CASE STUDY

This case study validates the fidelity of the aggregated model for system-wide applications, e.g. the dynamic security assessment solved by the TSOs. The grid is a modified New England 10-machine system with inclusions of 3 VPPs. Three SGs with nearby loads are replaced with the VPPs. The topology of the VPPs and the overall grid is shown in Fig. 12. For simplicity, the topology of each VPP is identical, but the capacities and parameters of the DGs are different (see Table III) as well as the distributed loads in the VPP.

For the detailed grid formulation, the GFL- and GFM-DGs are represented with full-order models [28], including the dynamics of voltage and current controllers and converter filters. The model of the SGs and their primary controls, i.e. AVRs and Turbine Governors (TGs), are given in [29].

This case study aims to verify the accuracy of the proposed aggregated model in different scenarios, namely, contingencies occurring at supply and demand buses as well as in the transmission system. The grid frequency is estimated with CoI. Finally, simulations are solved with Dome, a Python-based power system software tool [30].

The computation is carried out by the Dell Inspiron 15-3567 with 4 Intel Core i5-7200 U 2.5 GHz. The computational time of the full model is 35.267 s while that of the aggregated model is 26.582 s. There is a 24.6 % reduction on the computational time. This reduction can be further increased for the modern power system with increasingly high penetration of VPP.

A. Eigenvalue Analysis

Before doing the time domain simulation, this section compares the eigenvalue of the system using aggregated models with that using detailed VPP models.

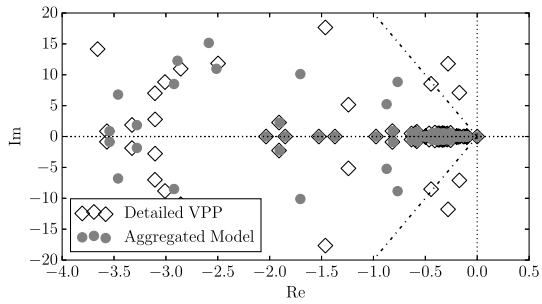

Fig. 13. Eigenvalue comparison between the detailed VPP and Aggregated Model.

Figure 13 shows the comparison results of the critical eigenvalues. Due to the simplicity, the aggregated model has less number of the eigenvalues, but the dominated or right most eigenvalues are well represented. However, the detailed VPP, due to the control interactions, presents extra a pairs of eigenvalues in the poor damped area, for example at -0.17207±j7.097100. This will lead to oscillations at the corresponding frequency, i.e. 2.42 Hz, as proved latter in Fig. 14b, Fig. 15b and Fig. 16b.

B. Scenario 1: Generator Outage

This scenario considers the outage of the machine Gen 8 at $t = 1$ s. Figure 14 shows the trajectories of the grid frequency, the active power and reactive power of the VPP 1 at its POC, and the voltages at the nearby grid buses.

The active power response of the VPP can be accurately captured by the aggregated model, as shown in Fig. 14b, so that the grid frequency response (see 14a) is identical to the one obtained with the detailed model. On the other hand, as expected, the reactive power, e.g. see Fig. 14d, obtained from the aggregated model shows a small mismatch with respect to that of the detailed VPP, thus, resulting in a small mismatch on the voltage response, as shown in Fig. 14c.

C. Scenario 2: Load Outage

This scenario considers the outage of the load at bus 8 at $t = 1$ s. To avoid repetitions, we only show the system frequency and bus voltages. After the contingency, since the generation is greater than the loading, the system frequency increases. The aggregated model accurately captures such a dynamic response of the frequency as well as the voltage response as shown in Fig. 15.

D. Scenario 3: Line Outage

This scenario considers the outage of the line connecting buses 2 and 25 at $t = 1$ s. Fig. 16 shows the system response obtained with the detailed and the proposed aggregated VPP models. In this case, the frequency response of the aggregated model presents a mismatch in the first 7 s after the contingency. This mismatch is due to the converter controller dynamics, whose dynamic effect is also shown in the EMT results discussed in Section IV. This mismatch, however, is very small in percentage

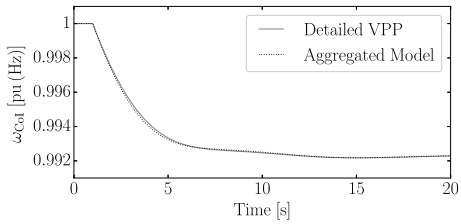

(a) System frequency.

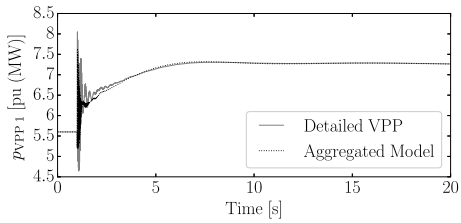

(b) VPP1 active power at POC.

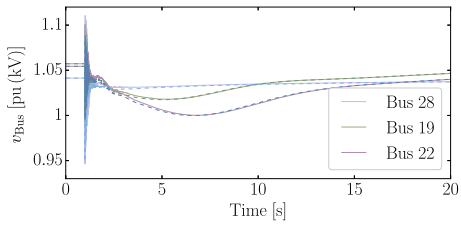

(c) Bus voltages.

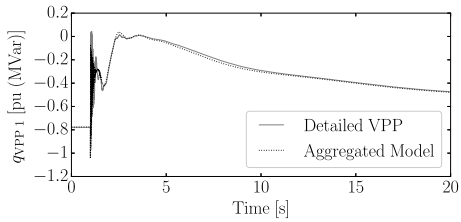

(d) VPP1 reactive power at POC.

Fig. 14. Modified New England system, Scenario 1: generator outage.

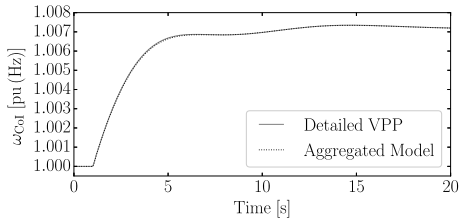

(a) System frequency.

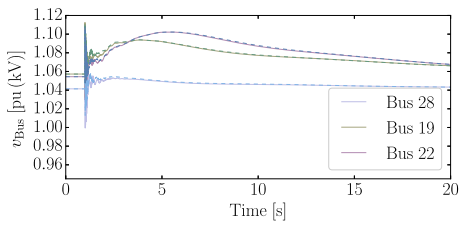

(b) Bus voltages.

Fig. 15. Modified New England system, Scenario 2: load outage.

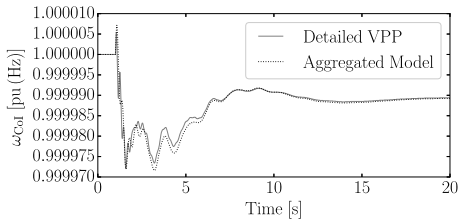

(a) System frequency.

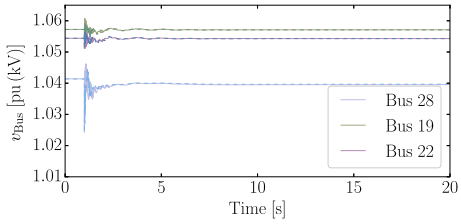

(b) Bus voltages.

Fig. 16. Modified New England system, Scenario 3: line outage.

and absolute values. It is visible only because of the small scale of the y-axis in Fig. 16a.

VI. Conclusion

This paper proposes an aggregated low-order model of VPP that is able to accurately capture the transient response of VPP with respect to the system contingencies. The proposed aggregated model consists of a current source to represent GFL-DG dynamics and a voltage source to represent GFM-DG dynamics in the VPP. Loads are also properly represented in the proposed aggregated model. Simulation results indicates that, with this model, TSOs can study the dynamic response of the grid without loss of accuracy and with no need to model in detail the network and the various units in the VPP. In the future work, the effect of the VPP system resistance on the damping coefficient of the aggregated model could be further investigated. Besides, based on this model, the secondary control of the VPP could also be aggregated, and then frequency and voltage stability in a national grid could be analyzed.

References

[1] E. Mashhour and S. M. Moghaddas-Tafreshi, "Bidding strategy of virtual power plant for participating in energy and spinning reserve markets-part I: Problem formulation," *IEEE Trans. Power Syst.*, vol. 26, no. 2, pp. 949–956, May 2011.

[2] G. Zhang, C. Jiang, and X. Wang, "Comprehensive review on structure and operation of virtual power plant in electrical system," *IET Gener., Transmiss. Distrib.*, vol. 13, no. 2, pp. 145–156, 2019.

[3] J. Rocabert, A. Luna, F. Blaabjerg, and P. Rodrguez, "Control of power converters in ac microgrids," *IEEE Trans. Power Electron.*, vol. 27, no. 11, pp. 4734–4749, Nov. 2012.

[4] J. Hu, L. Sun, X. Yuan, S. Wang, and Y. Chi, "Modeling of type 3 wind turbines with df/dt inertia control for system frequency response study," *IEEE Trans. Power Syst.*, vol. 32, no. 4, pp. 2799–2809, Jul. 2017.

[5] S. DArco, J. A. Suul, and O. B. Fosso, "A virtual synchronous machine implementation for distributed control of power converters in smartgrids," *Electric Power Syst. Res.*, vol. 122, pp. 180–197, 2015.

[6] D. Dong, B. Wen, D. Boroyevich, P. Mattavelli, and Y. Xue, "Analysis of phase-locked loop low-frequency stability in three-phase grid-connected power converters considering impedance interactions," *IEEE Trans. Ind. Electron.*, vol. 62, no. 1, pp. 310–321, Jan. 2015.
[7] J. Chen and T. O'Donnell, "Analysis of virtual synchronous generator control and its response based on transfer functions," *IET Power Electron.*, vol. 12, no. 11, pp. 2965–2977, 2019.
[8] Q. Shi, F. Li, and H. Cui, "Analytical method to aggregate multi-machine sfr model with applications in power system dynamic studies," *IEEE Trans. Power Syst.*, vol. 33, no. 6, pp. 6355–6367, Nov. 2018.
[9] H. Huang *et al.*, "Generic system frequency response model for power grids with different generations," *IEEE Access*, vol. 8, pp. 14 3 14–14 321, 2020.
[10] J. Dai, Y. Tang, Q. Wang, and P. Jiang, "Aggregation frequency response modeling for wind power plants with primary frequency regulation service," *IEEE Access*, vol. 7, pp. 108 561–108 570, 2019.
[11] M. G. Taul, X. Wang, P. Davari, and F. Blaabjerg, "Reduced-order and aggregated modeling of large-signal synchronization stability for multi-converter systems," *IEEE Trans. Emerg. Sel. Top. Power Electron.*, vol. 9, no. 3, pp. 3150–3165, Jun. 2021.
[12] H. Ye, W. Pei, and Z. Qi, "Analytical modeling of inertial and droop responses from a wind farm for short-term frequency regulation in power systems," *IEEE Trans. Power Syst.*, vol. 31, no. 5, pp. 3414–3423, Sep. 2016.
[13] J. Zhang and H. Xu, "Online identification of power system equivalent inertia constant," *IEEE Trans. Ind. Electron.*, vol. 64, no. 10, pp. 8098–8107, Oct. 2017.
[14] A. Tarkiainen, R. Pollanen, M. Niemela, and J. Pyrhonen, "Identification of grid impedance for purposes of voltage feedback active filtering," *IEEE Power Electron. Lett.*, vol. 2, no. 1, pp. 6–10, Mar. 2004.
[15] U. Rudez and R. Mihalic, "Analysis of underfrequency load shedding using a frequency gradient," *IEEE Trans. Power Del.*, vol. 26, no. 2, pp. 565–575, Apr. 2011.
[16] F. Drfler, J. W. Simpson-Porco, and F. Bullo, "Breaking the hierarchy: Distributed control and economic optimality in microgrids," *IEEE Control Netw. Syst.*, vol. 3, no. 3, pp. 241–253, Sep.2016.
[17] A. Yazdani, *"Voltage-Sourced Converters"* in *Power Systems Modeling, Control and Applications*. Hoboken, NJ, USA: Wiley, 2010.
[18] A. Luna *et al.*, "Grid voltage synchronization for distributed generation systems under grid fault conditions," *IEEE Trans. Ind. Appl.*, vol. 51, no. 4, pp. 3414–3425, Jul./Aug. 2015.
[19] Y. Tan, L. Meegahapola, and K. M. Muttaqi, "A suboptimal power-point-tracking-based primary frequency response strategy for DFIGS in hybrid remote area power supply systems," *IEEE Trans. Energy Convers.*, vol. 31, no. 1, pp. 93–105, Mar. 2016.
[20] Y. Li, Z. Xu, and K. P. Wong, "Advanced control strategies of PMSG-based wind turbines for system inertia support," *IEEE Trans. Power Syst.*, vol. 32, no. 4, pp. 3027–3037, Jul. 2017.
[21] L. Zhang, L. Harnefors, and H. Nee, "Power-synchronization control of grid-connected voltage-source converters," *IEEE Trans. Power Syst.*, vol. 25, no. 2, pp. 809–820, May 2010.
[22] L. Huang *et al.*, "A virtual synchronous control for voltage-source converters utilizing dynamics of dc-link capacitor to realize self-synchronization," *IEEE Trans. Emerg. Sel. Top. Power Electron.*, vol. 5, no. 4, pp. 1565–1577, Dec. 2017.
[23] S. D'Arco and J. A. Suul, "Equivalence of virtual synchronous machines and frequency-droops for converter-based microgrids," *IEEE Trans. Smart Grid*, vol. 5, no. 1, pp. 394–395, Jan. 2014.
[24] M. Liu, J. Chen, and F. Milano, "On-line inertia estimation for synchronous and non-synchronous devices," *IEEE Trans. Power Syst.*, vol. 36, no. 3, pp. 2693–2701, May 2021.
[25] F. Milano and À. Ortega, "A method for evaluating frequency regulation in an electrical grid - part I: Theory," *IEEE Trans. Power Syst.*, vol. 36, no. 1, pp. 183–193, Jan. 2021.
[26] Á. Ortega and F. Milano, "A method for evaluating frequency regulation in an electrical grid - part II: Applications to non-synchronous devices," *IEEE Trans. Power Syst.*, vol. 36, no. 1, pp. 194–203, Jan. 2021.
[27] J. Chen and T. O'Donnell, "Parameter constraints for virtual synchronous generator considering stability," *IEEE Trans. Power Syst.*, vol. 34, no. 3, pp. 2479–2481, May 2019.
[28] J. Chen, M. Liu, C. O'Loughlin, F. Milano, and T. O'Donnell, "Modelling, simulation and hardware-in-the-loop validation of virtual synchronous generator control in low inertia power system," in *Proc. Power Syst. Comput. Conf.*, 2018, pp. 1–7.
[29] F. Milano, *Power System Modelling and Scripting*., Berlin, Germany: Springer, 2010.
[30] F. Milano, "A python-based software tool for power system analysis," in *Proc. IEEE Power Energy Soc. Gen. Meeting*, 2013, pp. 1–5.

Muyang Liu (Member, IEEE) received the M.E. and Ph.D. degrees in electrical energy engineering from University College Dublin, Dublin, Ireland, in 2016 and 2019, respectively. Since December 2019, she has been a Senior Researcher with University College Dublin. Her current research interests include power system modeling and stability analysis. Her scholarship is funded through the SFI Investigator Award with title "Advanced Modeling for Power System Analysis and Simulation."

Junru Chen (Member, IEEE) received the M.E. and Ph.D. degrees in electrical energy engineering from University College Dublin, Dublin, Ireland, in 2016 and 2019, respectively. He was an Exchanging Student with Kiel University, Kiel, Germany, in 2018 and with the Tallinn University of Technology, Tallinn, Estonia. He is currently a Senior Researcher with University College Dublin and a Visiting Scholar with Aalborg University, Aalborg, Denmark. His current research interests include power electronics control, modeling, stability, and application.

Federico Milano (Fellow, IEEE) received the M.E. and Ph.D. degrees in electrical engineering from the University of Genoa, Genoa, Italy, in 1999 and 2003, respectively. From 2001 to 2002, he was with the University of Waterloo, Waterloo, ON, Canada. From 2003 to 2013, he was with the University of Castilla-La Mancha, Ciudad Real, Spain. In 2013, he joined University College Dublin, Dublin, Ireland, where he is currently a Professor of power systems control and protections and the Head of Electrical Engineering. His research interests include power systems modeling, control, and stability analysis.